Bioconjugate Chemistry

Article

pubs.acs.org/bc

Surface Chemistry Dependent "Switch" Regulates the Trafficking and Therapeutic Performance of Drug-Loaded Carbon Nanotubes

Manasmita Das,[†] Raman Preet Singh,[†] Satyajit R. Datir, and Sanyog Jain*

Centre for Pharmaceutical Nanotechnology, Department of Pharmaceutics, National Institute of Pharmaceutical Education and Research (NIPER), Sector 67, SAS Nagar (Mohali), Punjab, 160062, India

Supporting Information

ABSTRACT: The present study explores the possibility of exploiting surface functionality as one of the key regulators for modulating the intracellular trafficking and therapeutic performance of drug loaded carbon nanotubes (CNTs). In line with that approach, a series of biofunctionalized multiwalled carbon nanotubes (f-CNTs **1**−**6**) decorated with various functional molecules including antifouling polymer (PEG), tumor recognition modules (folic acid/hyaluronic acid/estradiol), and fluorophores (rhodamine B isothiocyanate/Alexa Fluor) were synthesized. By loading different anticancer agents (methotrexate (MTX), doxorubicin (DOX), and paclitaxel (PTX)) onto each functionalized CNT preparation, we tried to elucidate how the surface functional molecules associated with each f-CNT influence their therapeutic potential. We observed that antiproliferative or apoptotic activity of drug-loaded CNTs critically depends on their mechanistic pathway of cellular internalization and intracellular trafficking, which in turn had an intimate rapport with their surface chemistry. To our knowledge, for the first time, we have embarked on the possibility of using a surface chemistry dependent "switch" to remote-control the second and third order targeting of chemotherapeutic agents supramolecularly complexed/adsorbed on CNTs, which in turn is expected to benefit the development of futuristic nanobots for cancer theranostics.

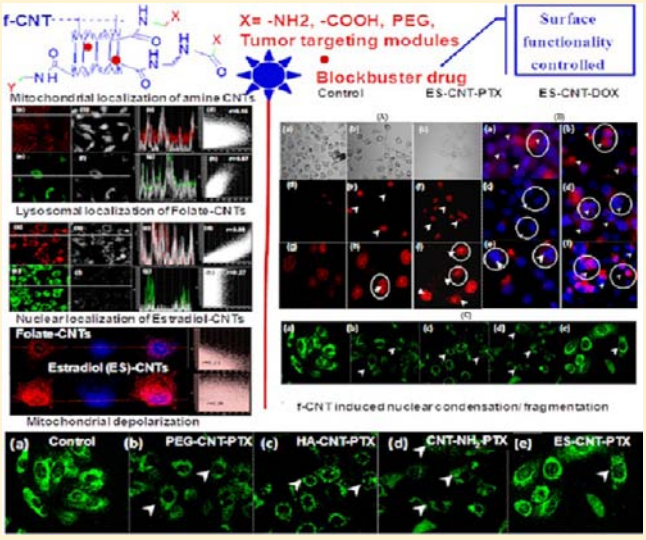

INTRODUCTION

In recent years, there has been an unprecedented flurry for the development of novel, multifunctional materials for theranostic applications. Among the myriad of nanocarriers that are able to augment the delivery, absorption, and intracellular uptake of bioactive molecules while protecting them from deactivation, functionalized carbon nanotubes (CNTs) have sparked significant interest. Their unique physicochemical properties, especially high surface area and pseudoaromatic structure, render these nanoscale materials extremely versatile through the incorporation of multiple diagnostic and therapeutic entities on the same nanotube platform while their fluorescence detectability and photoacoustic effects make them a potential asset in the armory of theranostic nanocarriers.[1−3] The interaction between cells and CNTs is a critical issue that determines the future applicability of these theranostic materials. Unfortunately, much about the interaction of CNTs with living cells is still an unraveled mystery. Furthermore, current published data of cellular uptake and toxicity of functionalized CNTs are particularly inconsistent and an issue of debate. As reported in a number of studies, the natural shape of CNTs allows their noninvasive penetration across biological barriers through an energy-independent, "nanoneedle" mechanism.[4] This unique property of CNTs facilitates the transport of a wide variety of cargos inside phagocytic and nonphagocytic cells that otherwise would have been difficult. While many researchers attributed "nanoneedle" mechanism to be the predominant pathway of nanotube internalization inside the cells, others continue to focus on energy dependent, endocytosis-based mechanisms critically influenced by the functional molecules attached to the surfaces of CNTs[5−12]. As evident from an extensive literature survey, cellular uptake and cytotoxic responses of CNTs to living cells depend on a number of critical parameters that include nanotube length, degree of aggregation (and aggregate dimensions), and surface coat/density of functional ligands associated with CNTs. Especially, when we are talking about functionalized CNTs, the nature of the functional groups covalently linked or noncovalently complexed to the CNTs seems to be of great importance. It is possible that the

Received: November 9, 2012
Revised: February 19, 2013
Published: March 21, 2013

 © 2013 American Chemical Society

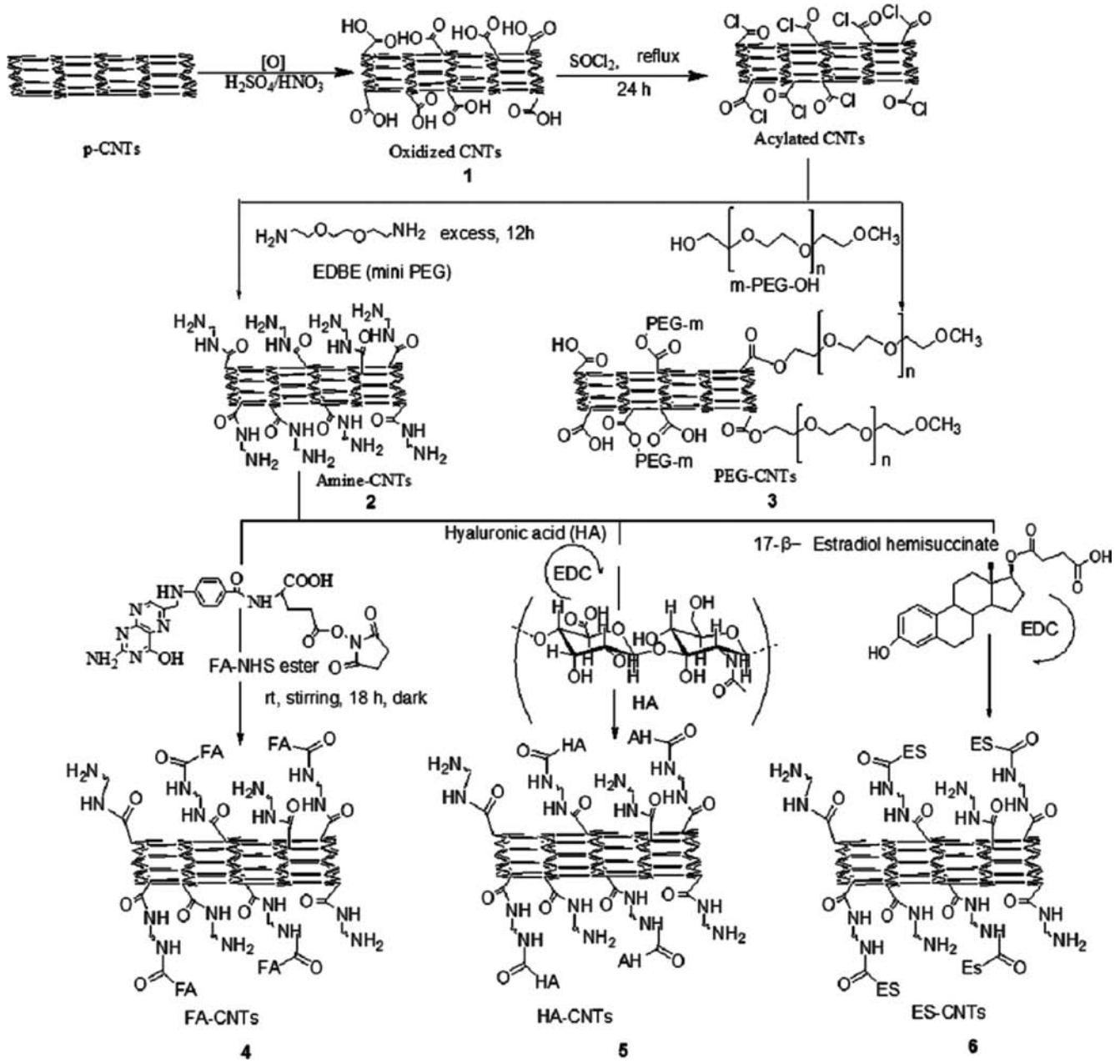

Figure 1. Schematic representation illustrating the biofunctionalization of CNTs.

functional molecules or ligands present on the surface of CNTs impede their direct interactions with cell membrane, rendering the tubes impermeable through plasma membrane. In this context, the functional molecules present on CNTs play a crucial role, as these ligands may bind to extracellular receptors that recognize them as ligands and expedite their cellular internalization through receptor mediated endocytosis. This explanation is also consistent with the findings of our recently published report in which hyaluronic acid present on the surface of CNTs triggered the active process of cellular internalization through receptor mediated endocytosis.[13] In the course of our past few years' endeavor to come up with new multifunctional CNTs for theranostic applications, we observed that the efficacy of any cytotoxin loaded on CNTs critically depends on their surface coat and cell type. While a number of studies have dealt with the design, fabrication, and biological evolution of drug loaded CNTs, the fundamental point of whether and how the conjugation of one or more functional molecules influences the targeting and therapeutic index of any drug molecule(s) supramolecularly complexed/physically adsorbed on CNTs still remains unaddressed. The present study in part was motivated by an urge to elucidate whether surface functionality can be used as a "regulator" to modulate the therapeutic performance of drug loaded CNTs. In line with that approach, we prepared a series of biofunctionalized multiwalled carbon nanotubes (MWCNTs) decorated with various functional molecules including antifouling polymer (PEG) and tumor recognition modules (folic acid (FA), hyaluronic acid (HA), and estradiol (ES)). Three different anticancer agents, methotrexate (MTX), doxorubicin (DOX), and paclitaxel (PTX), were loaded onto each functionalized CNT preparation, and their cytotoxic potential was evaluated in three different cancer cell lines of different origin. We observed that cytotoxic responses to drug loaded CNTs critically depend on

their mechanistic pathway of cellular internalization and intracellular trafficking, which in turn had an intimate rapport with the surface chemistry of CNTs.

■ MATERIALS AND METHODS

Materials. Pristine (p) MWCNTs (purity of >95%, length of 1−2 μm, and diameter of 20−30 nm) were procured from Nanovatech Pvt. Ltd., U.S. Throughout the description, MWCNTs have been designated as "CNTs", unless otherwise specified. Sulfuric acid, nitric acid (69−72%), *N*-hydroxysuccinimide (NHS), 1-ethyl-3-(3-dimethylaminopropyl)-carbodiimide (EDC), disodium hydrogen phosphate, sodium acetate, thionyl chloride, sodium lauryl sulfate, copper sulfate, and thiobarbituric acid were purchased from Loba Chemie Pvt. Ltd., Mumbai, India. MTX and HA acid were obtained as gift samples from Fresenius Kabi Oncology Limited, Gurgaon, India, and Focaschem Biotech Limited, China, respectively. 2,2′-(Ethylenedioxy)bis(ethyleneamine) (EDBE), folic acid, estradiol, succinic anhydride, glycidol, 3-(4,5-dimethylthiazol-2-yl)-2,5-diphenyltetrazolium (MTT), propidium iodide (PI), 4′,6-diamidino-2-phenylindole dihydrochloride (DAPI), rhodamine isothiocyanate (RITC), and annexin V/Cy3 were purchased from Sigma, U.S. Culture medium and serum were procured from PAA, Austria. Human lung (A549), cervical (HeLa), and breast (MCF) carcinoma cells were obtained from the National Centre for Cell Sciences (NCSS), Pune, India. Maleimide ester of Alexa-Fluor 647 (AF-647) was purchased from Invitrogen, U.S. All other chemicals and solvents were of analytical grade and procured from local suppliers unless otherwise mentioned.

Functionalization of CNTs. *Preparation of f-CNTs **1**−**6**.* The chemical synthesis of f-CNTs **1**−**6** used in this study has been schematized in Figure 1.

*Preparation of Oxidized (Carboxyl) CNTs (**1**).* Acid-oxidized carboxylated CNTs (**1**) were prepared via surface oxidation as described in our earlier reports.[14−16] Briefly, pristine CNTs (200 mg) with approximate length ranging from 1 to 2 μm and diameter of 20−30 nm were dispersed in a 3:1 (v/v) mixture of H_2SO_4/HNO_3 (20 mL) via ultrasonication for 5 min. Subsequently, the dispersion was refluxed at 80 °C using a hot plate with magnetic stirrer at 900 rpm. The reaction mixture was heated for 3 h. Thereafter, the suspension of oxidized CNTs in acid was diluted up to 5 times its volume and centrifuged at 21 000 rpm. This washing was repeated thrice for complete removal of acid. The resultant oxidized CNTs were further dispersed in acetone and centrifuged. Finally, the supernatant was discarded and CNTs were air-dried for approximately 12 h to obtain fine powders of oxidized CNTs[17] in quantitative yield. Yield, ∼95% w/w.

*Preparation of Amine CNTs (**2**).* The carboxyl functions of oxidized CNTs (**1**) were interchanged with EDBE to produce the amine functionalized CNTs, **2**.[13] From thermogravimetric analysis (TGA), the carboxylic density on the surface of **1** was determined to be 0.0018 mmol/mg CNTs. This value was essential for calculating the exact amount of EDBE that would be ideally required for complete amination of surface carboxyl groups. Briefly, oxidized CNTs (100 mg) were dispersed in THF (10 mL) via ultrasonication for 1 min. To the resultant dispersion, $SOCl_2$ (15−20 mL) was added and the mixture was refluxed at 80 °C for 24 h.[18] Thereafter, solvents were removed using rotavapor and the resultant acylated CNTs. Around 3-fold molar excess of EDBE (0.810 μg/mg oxidized CNTs) was dissolved in anhydrous DMSO (1 mL) and added to a suspension of acylated CNTs dispersed in a 5:1 (v/v) mixture of DMSO and pyridine under ice cold conditions. The reaction mixture was left stirring for 12 h, after which the reaction mixture was subjected to centrifugation, the supernatant was discarded, and the pellet of amine-CNTs was washed with distilled water, recentrifuged to remove the unreacted reagents, and dried by repeated washing with acetone. Yield, ∼95% w/w.

*Preparation of PEG-CNTs (**3**).* For preparation of PEGylated CNTs, carboxylated CNT **1** (100 mg) was acylated using the same protocol as described above and reacted with m-PEG 3500 for 24 h to afford the PEGylated conjugate **3** (Figure 1). The purification steps adopted for **3** were same as in case of **2**. Yield, ∼85% w/w).

*Preparation of FA-CNTs (**4**).* As a preliminary step toward the conjugation of FA with **2**, *N*-hydroxysuccinimide (NHS) ester of FA was prepared using standard carbodiimide chemistry, following our previously reported protocol.[19,20] Subsequently, FA-NHS ester (8.32 μmol) was dissolved in freshly distilled DMSO (1 mL) and added to a suspension of f-CNTs (20 mg) in water (5 mL). After being stirred for 24 h in dark, the reaction mixture was subjected to centrifugation and the supernatant was discarded. The pellet of FA-CNTs (**4**) was washed with distilled water, recentrifuged to remove the unreacted FA-NHS, and freeze-dried using a previously optimized, stepwise freeze-drying process patented by our group (Indian patent application 2559/DEL/2011).

*Preparation of HA-CNTs (**5**).* HA tethered CNTs (**5**) were prepared using our recently published procedure.[13] Briefly, HA (taken in a concentration equivalent to the surface amine density of **2**) was dissolved in water at pH 8.0 and activated with NHS and EDC·HCl for 6 h. To this activated HA, an aqueous suspension of **2** was added and the reaction mixture was stirred for 24 h. Subsequently, HA-EDBE-CNTs were separated and air-dried for 12 h (yield, ∼80% w/w).

*Preparation of ES-CNTs (**5**).* For preparation of estradiol functionalized CNTs **6**, β-estradiol-17-hemisuccinate was reacted with amine-CNTs (**2**) using the same procedure used for coupling of FA with **2**. Briefly, hemisuccinate of β-estradiol was activated with NHS/EDC in DMSO using standard carbodiimide chemistry. Following reaction for 24 h, the pellet of ES-CNTs (**6**) was collected by centrifugation, washed repeatedly (3−4 times) with water and acetone to remove the unreacted starting materials/biproducts, and freeze-dried.

Fluorescent Labeling of f-CNTs with RITC/AF-647. Aqueous suspensions of f-CNTs **1**−**6** (20 mg dispersed in 5 mL of water) were added separately to RITC and amine reactive NHS ester of AF-647 (∼1 μmol) and dissolved in DMSO (1 mL) and tetrahydrofuran (THF, 1 mL). In either case, catalytic amount of triethyl amine (Et_3N) was added to maintain the pH of the reaction mixture near 8. Thereafter, the suspension was stirred for 2 h in dark, after which fluorescently labeled nanotubes were separated by centrifugation, washed 4−5 times with distilled water, recentrifuged to remove the unreacted dye, and used for subsequent studies.

Drug Loading on f-CNTs. Doxorubicin was loaded onto pristine (p-) and f-CNTs (**1**−**6**) via π−π stacking at physiological pH (7.4) as described in our recently published report.[13] Briefly, HA-CNT and DOX were mixed in the ratio of 2:1 (w/w), and the resultant mixture was incubated at pH 7.4. The CNT−drug mixture was kept in a shaker bath at 37 °C for 24 h, after which the drug loaded CNTs were separated by centrifugation and absorbance of the supernatant was measured at 480 nm. For MTX loading, the drug was dissolved in DMSO

(1 mL), after which the MTX solution and the various f-CNTs (suspended in 10 mL of water) were mixed in a ratio of 1:2 (w/w). The pH of the suspension was adjusted to be between 5.5 and 6.0 using 0.01 M acetic acid (CH_3COOH). Subsequently, the f-CNT-drug mixtures were kept in a shaker bath at 37 °C for 24 h, after which the drug loaded CNTs were separated by centrifugation and absorbance of the supernatant was measured at 302 nm. Compared to DOX or MTX, PTX has much lower solubility in aqueous solution and has no extended π-structures larger than one aromatic ring. PTX loading on p-/f-CNTs was executed by physical loading of PTX onto the side walls of CNTs using the procedure adopted by Lay et al.[21] Briefly, a saturated solution of PTX in 1 mL of methanol was mixed with 20 mg of each f-CNT preparation. The mixture was ultrasonicated for 0.5 h and subjected to stirring for an additional 6 h. Thereafter, the pellets of drug-loaded f-CNTs were collected by centrifugation and dried under vacuum at 30 °C. The dried solid was dispersed in 5 mL of deionized water under ultrasonication for 5 min and subjected to lyophilization. MTX and DOX loading was calculated spectrophotometrically using the following formula, % drug encapsulation efficiency = $[(A_1 - A_2)/A_1] \times 100$, where A_1 is the free DOX/MTX absorbance and A_2 is the absorbance of supernatant after centrifugation. Drug content (%) was estimated as % drug content = [(amount of drug encapsulated)/(weight of the pellet)] × 100. To measure the content of PTX in f-CNTs, an amount of 5 mg of drug loaded f-CNTs was dissolved in 1 mL of dichloromethane (DCM) under ultrasonication for 30 min. After DCM was evaporated at room temperature, the residual solid was redissolved in 2 mL of a 50:50 (v/v) mixture of acetonitrile and water under ultrasonication for 30 min. Drug content was measured by HPLC analysis using our previously reported method.[18]

Physicochemical Characterization of f-CNTs 1−10. Size and morphology of f-CNTs were analyzed using transmission electron microscopy (TEM, model FEI Tecnai G2), while ζ potential measurements were carried out using the Malvern Zeta Sizer (Nano ZS, Malvern Instruments, U.S.). Surface chemistry of the functionalized nanotubes was preliminarily studied using Fourier transform infrared (FTIR), while fine-structure resolved analysis of the surface bound ligands was performed using high resolution magic angle spinning NMR (HRMAS-NMR) spectroscopy. FTIR spectra were recorded on Perkin-Elmer systems using KBr pellets and processed using Spectrum Software. Samples for MAS experiments were prepared by suspending 10 mg of each nanoparticle preparation in a 1:1 mixture of DMSO-d_6/D_2O (500 μL).[22] HRMAS-NMR analysis was carried out with a 400 MHz FT-NMR spectrometer (Avance 400) equipped with a 5 mm HRMAS probe.

Quantification of Different Functional Molecules on f-CNTs. Carboxyl density on the surface of f-CNT **1** was calculated by TG analysis, as described in our earlier reports. The stoichiometry of the amine functionalization step was chosen based on the availability of the $-CO_2H$ group per unit mass of CNTs. The number of free amine groups on **2** was quantified using *p*-nitrobenzaldehyde colorimetric assay.[23] The quantity of FA coupled on **4** was determined using our previously published protocol.[24] Briefly, FA-CNTs, **4**, were digested with trypsin at 37 °C for 12 h under continuous stirring. Following tryptic hydrolysis of FA-conjugated CNTs, the folate density on CNTs was determined spectrophotometrically by recording the absorbance of hydrolyte at 358 nm (folic acid ε = 8643.5 M^{-1} cm^{-1}). The number of HA and estradiol conjugated per unit mass of CNTs was determined by calculating the residual amine concentrations on the surfaces of **5** and **6** using *p*-nitrobenzaldehyde assay.[13]

In Vitro Drug Release from f-CNTs. The release behavior of MTX and DOX from f-CNTs was checked at two different pH conditions: pH 7.4 phosphate buffered saline (15 mmol) and pH 5.5 acetate buffered saline (15 mmol) to mimic the physiological and lysosomal pH, respectively. Briefly, an aqueous dispersion of drug loaded CNTs (5 mg dispersed in 2 mL of water) was filled in the dialysis membrane (MW CO, 12 000 Da), poured into release medium (15 mL), and placed inside the water shaker bath for 48 h at 37 °C and 1200 rpm. Aliquots were taken at periodic intervals up to 48 h, and absorbance was recorded using UV spectroscopy at 302 and 480 nm, respectively. For quantification of PTX release, stock solutions (500 mL) of 1:1 (v/v) mixture of methanol and phosphate buffer (pH 7.4 and pH 5.5, respectively) were prepared following the procedure depicted in United States Pharmacopeia, 28th revision (USP XXVIII). Subsequently, 10 mg of each PTX-loaded f-CNT preparation was dispersed in 2 mL of 1:1 (v/v) mixture of methanol and phosphate buffer and filled inside the dialysis membrane (MW CO, 12 000 Da). CNT-filled dialysis bags were suspended in 10 mL of 1:1 (v/v) mixture of methanol and phosphate buffer at 37 °C under constant stirring. At different time intervals, 0.5 mL of the aliquot was withdrawn from the mixture and replaced with an equivalent amount of the release medium. The aliquot was centrifuged, and the supernatant was analyzed for PTX content using HPLC analysis.

In Vitro Cellular Uptake, Cytotoxicity, and Apoptosis Studies. *Cell Culture.* Cell uptake studies were conducted in three different cell lines: human non-small-cell lung carcinoma (A549), human cervical carcinoma (HeLa), and human breast adenocarcinoma (MCF7) cell lines. Cells (1×10^4 cells/well) were grown in Dulbecco's modified Eagle medium (DMEM) supplemented with 10% (v/v) fetal bovine serum, 2 mM glutamine, 100 units/mL penicillin, 100 μg/mL streptomycin, and 4 mmol/L glutamine at 37 °C in a 5% CO_2 and 95% air humidified atmosphere. Confluent cultures were harvested by trypsinization, and cells were counted and suitably diluted to obtain 5×10^5 cells/mL. Cell suspension (200 μL) was added in 96-well tissue culture plates and incubated overnight for cell attachment.

Cellular Uptake and Colocalization Studies. For evaluation of intracellular uptake, cultured cells were initially exposed to 10 μg/mL RITC-labeled f-CNTs for 3 h, after which the culture medium was removed and cells were lyzed (200 μL of 0.1% Triton X-100). The cell lysates were sonicated for 2−3 min to aid dispersion of CNTs. The concentrations of f-CNTs in the cell lysates were determined spectrophotometrically as described in one of our recently published reports.[15] The optical density of CNTs was measured at 560 nm, and concentrations of CNTs were determined from a standard plot. To understand how surface functionalities of f-CNTs influence their mechanism of cell internalization, A549 cells were incubated with RITC labeled f-CNTs (5, 10, and 20 μg/mL) in the absence and presence of excess sodium azide (NaN_3) (50 and 100 μg/mL) at 37 °C for 3 h. To check whether any specific receptor is involved in the cellular internalization of ligand anchored CNTs (**4**−**6**), A549 cells were incubated with FA, HA, and ES conjugated CNTs (**4**−**6**) in the absence and presence of FA, HA, and ES. Following 3 h of incubation, the

Table 1. Cellular Uptake and Internalization of Various f-CNTs[a]

p-/f-CNT[1]	Functionality present	Functionalization density *	Cell type	Confocal images
Pristine	-	-	A549 **HeLa** MCF7	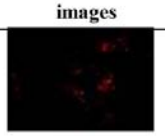
1	-COOH	1.8[2]	**A549** HeLa MCF7	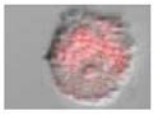
2	$-NH_2$	0.454	A549 **HeLa** MCF7	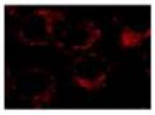
3	m-PEG	ND	**A549** HeLa MCF7	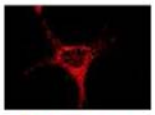
4	FA	0.234[2]	A549 **HeLa** MCF7	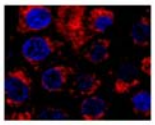
5	HA	0.218[2]	A549 **HeLa** MCF7	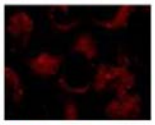
6	Estradiol	0.258	A549 HeLa **MCF7**	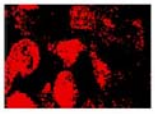

[a](*) Functionalization density expressed as μmol/mg. (1) f-CNTs labeled with RITC. (2) Carboxyl (−COOH) density was determined by TG analysis. Surface functionalization density of folic acid (FA) was determined by tryptic hydrolysis of FA-CNTs followed by spectrophotometric determination of the hydrolyte at 358 nm. The amount of hyaluronic acid (HA) and estradiol (ES) present per unit mass of CNTs was measured by determination of residual amine concentration using *p*-nitrobenzaldehyde assay.

cells were washed to remove the free noninternalized CNTs. The interaction of f-CNTs with their target cells was visualized by confocal microscopy [model Olympus FV 1000], while intracellular concentration of the nanotubes was determined spectrofluorometrically using a Nanodrop fluorospectrometer. Ligand−receptor interaction of selected nanotube preparations (e.g., FA-CNTs) was also assessed by flow cytometry in addition to confocal microscopy and spectrofluorometry. Intracellular colocalization studies were performed by labeling lysosomes, mitochondria, and nuclei of A549/HeLa/MCF7 cells with neutral red (NR), Rh123, and DAPI, respectively, as detailed in our earlier reports.[14,24]

In Vitro Cellular Cytotoxicity and Apoptosis Studies. f-CNT-induced cytotoxicity in A549, HeLa, and MCF7 cells was determined according to our previously published protocol.[25] The induction of apoptosis in A549 cells was determined by phosphatidylserine externalization (annexin V staining) and DNA fragmentation (TUNEL assay) after a 24 h incubation, using commercial assay kits and following the manufacturer's instructions. In A549 cells, nuclear morphology was assessed after a 24 h incubation with respective CNTs. Cells were fixed in 70% ethanol and stained with 10 μg/mL PI. DNA fragmentation was determined by the diphenylamine (DPA) method as described elsewhere.[26,27] In HeLa cells, apoptosis was studied qualitatively by monitoring the changes in nuclear morphology, following f-CNT treatment. Mitochondrial depolarization was studied qualitatively through rhodamine 123 staining.[28]

Statistical Analysis. All data unless otherwise specified are expressed as the mean ± SD. Statistical analysis was performed with GraphPad Prism software (version 4.03, U.S.) using one-way ANOVA, followed by Tukey−Kramer multiple comparison test. $P < 0.05$ was considered as statistically significant.

■ RESULTS AND DISCUSSIONS

Biofunctionalization of CNTs. The functionalized nanotubes used in the present study were prepared by carboxyl enrichment of pristine CNTs, followed by further functionalization with antifouling agents, fluorescent dyes, and tumor targeting modules. Using acid-oxidized carboxylated CNTs (**1**) as the bioconjugating precursor, we prepared five different CNT formulations wherein the surface of nanotubes was tethered with one or more chemical entities having distinct biological functions. The molecular structures and chemical synthesis of functionalized CNTs used in this study have been schematized in Figure 1. Covalent functionalization of CNTs was carried out in a modular fashion, i.e., by gradually increasing the complexity of the functional groups covalently immobilized onto the nanotube sidewalls. The simplest f-CNT investigated in this study was an amine functionalized CNT preparation (**2**) prepared by interchanging the carboxyl groups of acid-oxidized CNTs with a nonpolymeric and hydrophilic

Table 2. Half-Maximal Inhibitory Concentration (IC_{50}) of Free Drug and Drug Loaded f-CNTs

S/no.	formulation tested (drug/f-CNT)	drug loading		half-maximal inhibitory concn IC_{50} (μg/mL)[a]		
		entrapment efficiency (%)	drug content (%)	A549	HeLa	MCF7
1	MTX			7.0 ± 0.8	7.1 ± 0.8	6.9 ± 0.3
2	p-CNT-MTX (i)	98.3 ± 1.9	32.7 ± 0.6	7.9 ± 0.4	6.9 ± 0.2	6.3 ± 0.2
3	CNT-COOH-MTX (ii)	99.1 ± 0.6	33.2 ± 0.2	5.6 ± 0.2	6.3 ± 0.3	5.2 ± 0.2
4	CNT-NH_2-MTX (iii)	94.6 ± 1.2	32.2 ± 0.4	4.9 ± 0.3	4.8 ± 0.2	4.9 ± 0.4
5	CNT-PEG-MTX (iv)	93.7 ± 2.6	31.2 ± 0.8	5.1 ± 0.3	5.3 ± 0.4	4.5 ± 0.3
6	CNT-FA-MTX (v)	97.8 ± 2.1	32.6 ± 1.7	1.5 ± 0.3	1.2 ± 0.2	1.4 ± 0.3
7	CNT-HA-MTX (vi)	93.9 ± 3.4	31.3 ± 1.1	1.8 ± 0.2	1.4 ± 0.3	1.7 ± 0.4
8	CNT-ES-MTX (vii)	94.5 ± 2.2	31.5 ± 0.7	1.3 ± 0.2	2.5 ± 0.4	1.2 ± 0.3
9	DOX			2.7 ± 0.3	2.4 ± 0.3	2.6 ± 0.2
10	p-CNT-DOX (viii)	98.9 ± 0.6	32.6 ± 0.2	4.2 ± 0.4	4.9 ± 0.3	5.2 ± 0.2
11	CNT-COOH-DOX (ix)	99.3 ± 0.5	31.1 ± 0.1	2.4 ± 0.4	2.7 ± 0.3	2.6 ± 0.4
12	CNT-NH_2-DOX (x)	94.5 ± 0.7	31.5 ± 0.2	2.6 ± 0.3	2.1 ± 0.2	2.0 ± 0.3
13	CNT-PEG-DOX (xi)	93.9 ± 1.9	31.3 ± 0.6	1.8 ± 0.2	1.9 ± 0.2	1.5 ± 0.2
14	CNT-FA-DOX (xii)	97.8 ± 2.4	32.7 ± 0.8	1.1 ± 0.2	0.7 ± 0.2	0.9 ± 0.1
15	CNT-HA-DOX (xiii)	93.4 ± 3.2	31.1 ± 1.1	0.7 ± 0.1	1.0 ± 0.1	0.7 ± 0.1
16	CNT-ES-DOX (xiv)	97.5 ± 4.3	32.4 ± 1.4	0.6 ± 0.1	1.0 ± 0.2	0.6 ± 0.1
17	PTX			8.2 ± 0.2	8.4 ± 0.9	8.7 ± 0.9
18	p-CNT-PTX (xv)	98.8 ± 0.8	32.4 ± 0.2	7.3 ± 0.7	7.9 ± 0.1	6.9 ± 0.6
19	CNT-COOH-PTX (xvi)	94.6 ± 1.4	31.5 ± 0.7	4.8 ± 0.4	5.0 ± 0.1	5.0 ± 0.5
20	CNT-NH_2-PTX (iii)	93.1 ± 2.8	31.0 ± 0.9	3.3 ± 0.0	1.1 ± 0.1	3.7 ± 0.3
21	CNT-PEG-PTX (iv)	92.3 ± 3.5	30.1 ± 1.4	1.2 ± 0.1	3.6 ± 0.2	1.2 ± 0.2
22	CNT-FA-PTX (v)	91.4 ± 2.6	30.1 ± 1.3	2.5 ± 0.2	2.5 ± 0.2	2.4 ± 0.2
23	CNT-HA-PTX (vi)	92.5 ± 4.3	31.1 ± 1.4	1.1 ± 0.2	1.0 ± 0.1	1.1 ± 0.1
24	CNT-ES-PTX (vii)	95.6 ± 1.2	31.8 ± 1.2	2.7 ± 0.2	2.5 ± 0.1	2.6 ± 0.2

[a]Data represent the mean ± SEM of three experiments (n = 3 per concentration per experiment).

bisamine. Following a similar paradigm, PEGylated CNTs (**3**) were prepared by reacting acylated CNTs with a heterobifunctional, methoxy-terminated PEG. Molecular complexity of the surface was further increased by coupling free amine groups of **2** with tumor targeting modules, selected from the class of a vitamin (folic acid, FA), naturally occurring glycosaminoglycan (hyaluronic acid, HA), and steroidal hormone (estradiol, ES). The conjugation of FA, HA, and ES with **2** produced the conjugates **4**−**6** in conspicuous yield. Representative TEM images of selected f-CNTs with length ranging between 400 and 700 nm compared to the aggregated, pristine material have been depicted in Figure S1 (see Supporting Information). The immobilization of various functional molecules on **1** was authenticated using FTIR and high resolution magic angle spinning NMR (HRMAS-NMR) spectroscopy (see Supporting Information Figures S2 and S3 for selected spectral data). Three different anticancer agents methotrexate, doxorubicin, and paclitaxel were loaded on pristine as well as each f-CNT preparation to generate a small library comprising 21 different drug-loaded CNTs (i−xxi). The amount of different functional molecules associated with each CNT preparation is summarized in Table 1. The entrapment efficiency and practical loading (% w/w) of each f-CNT preparation are summarized in Table 2. In almost all cases, the efficiency of drug entrapment was higher than 90% and the practical loading ranged between 30% and 33%. In accordance with other studies that used differently functionalized CNTs,[4] both pristine (p-) and f-CNTs (**1**−**6**) were detected to be intrinsically luminescent in the ultraviolet or visible region. Meanwhile, pristine/f-CNTs (**1**−**6**) were supramolecularly complexed/covalently conjugated with maleimide ester of AF-647 or RITC to obtain high fluorescence signals for intracellular imaging.

In Vitro Drug Release from f-CNTs. The release profile of any drug−carrier combination is crucial for determining their clinical efficacy. Following their internalization into target cells, a drug, first of all, has to detach from the carrier in order to exert therapeutic effects. In this regard, it may be noted that the intracellular milieu is pretty complex, as differential pH and chemoenzymatic conditions prevail in the various intracellular compartments. For example, the cytosolic pH is neutral to mildly alkaline (7.4−7.8) whereas lysosomal pH is acidic (4−5.5). Similarly, a wide variety of cellular proteases and esterase are present inside various cellular compartments. The activity of these enzymes critically depends on the chemical constitution of the substrate. Therefore, for a drug molecule, which releases more quickly at cytosolic pH, it will be particularly beneficial if the carrier-bound drug is localized in the cytoplasm. Similarly, for a formulation that shows faster release rate under acidic conditions, it will be advantageous to have the carrier−drug combination localized in lysosomes. Subsequently, the release profiles of MTX, PTX, and DOX from f-CNTs (**1**−**6**) were studied at pH 7.4 (cytosolic pH) and pH 5.5 (lysosomal pH). As is evident from Figure S4, drug release from nanotubes critically depended on pH and/or solubility of the drug in a particular medium. In the case of DOX [Figure S4(a,b)], only 15−20% of the drug was released from the different CNT preparations at pH 7.4 following 48 h of incubation. As the pH of the medium was lowered to 5.5, drug release was increased to 45−55%, suggesting that DOX will be released more in acidic tumor sites than in the normal tissues. This particular release behavior will be even more beneficial if the f-CNTs, following their cellular internalization, traffick intracellularly to lysosomes. In that case, the lower pH value of lysosomes will augment drug release inside the acidic tumor endosomes. At this low pH, the hydrophilicity of DOX increases because of the

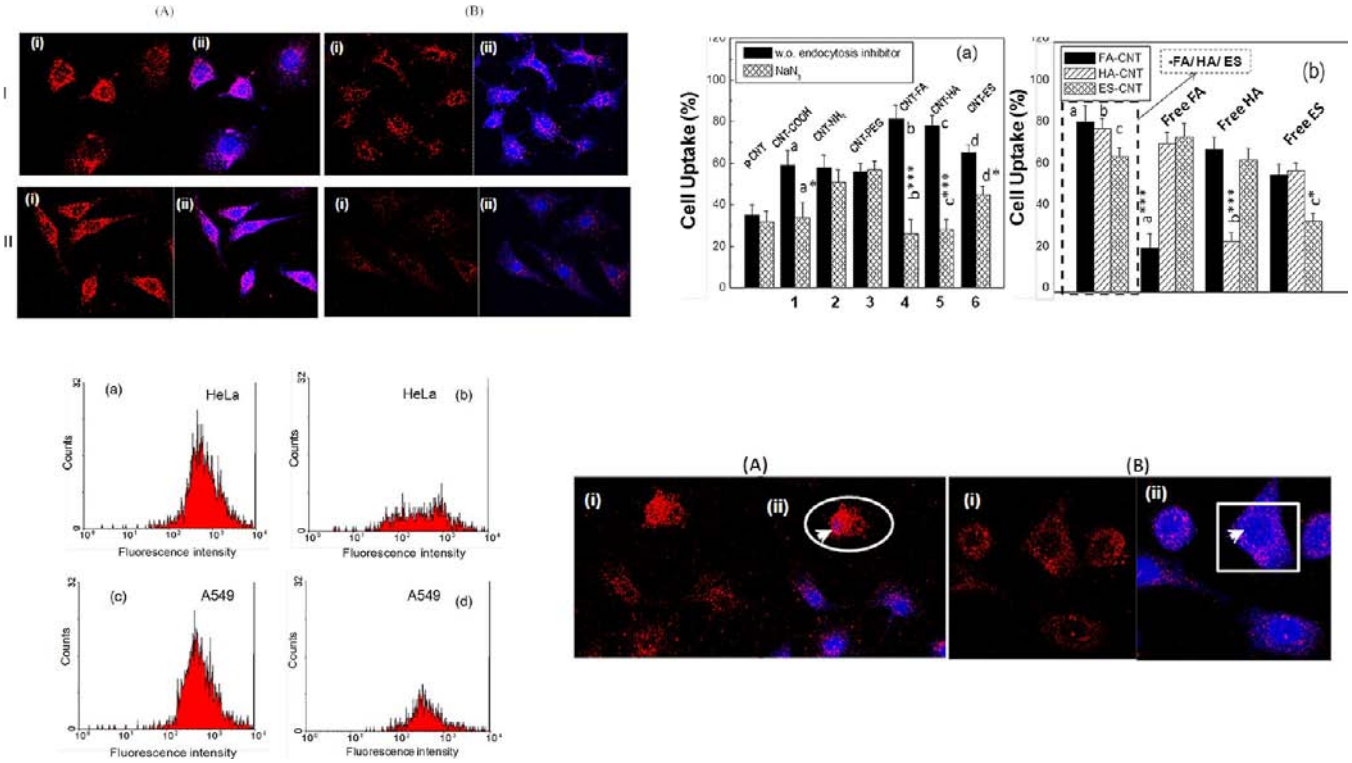

Figure 2. (A, upper-left) Confocal images of A549 cells treated with (I) amine-CNTs (**2**) and (II) folate CNTs (**4**). For each incubation type, the left portion (i) represents RITC fluorescence while the right portion (ii) represents overlay of RITC and DAPI fluorescence. The quadrants A and B represent incubation in the absence and presence of endocytosis inhibitor (NaN_3) respectively. (B, upper right) Quantification of cellular uptake of f-CNTs in the absence and presence of endocytosis inhibitors: (a) uptake profile of f-CNTs in A549 cells incubated with RITC-labeled f-CNTs in the absence and presence of NaN_3; (b) uptake profile of f-CNTs in A549 cells incubated with RITC-labeled f-CNTs in the absence and presence of targeting ligands. In (a), a*, b*, c*, and d* represent uptake with respect to CNT-COOH, CNT-FA, CNT-HA, and CNT-ES, respectively. In (b), a*, b*, and c* represent uptake with respect to CNT-FA, CNT-HA, and CNT-ES, respectively ((***) $p < 0.001$, (**) $p < 0.01$, (*) $p < 0.05$). (C, lower-left) Representative flow cytogram of (a, b) HeLa and (c, d) A549 cells treated with FA-CNTs, **4**, in the absence and presence of free folic acid. The left and right panels represent incubation in the absence and presence of FA, respectively. A significant depreciation in fluorescence intensity was observed for FA pretreated cells, suggesting competitive inhibition of **4** by free FA. (D, lower-right) Representative confocal images of A549 cells treated with estradiol-CNTs (**6**) in the absence (A) and presence (B) of free estradiol. For incubation type (A, left two panels) the white circle indicates nuclear colocalization of nanotubes whereas for (B) (right two panels) the square represents the clear nuclear zone. For each incubation type, (i) and (ii) represent the RITC fluorescence and overlay of RITC and DAPI fluorescence, respectively.

protonation of the NH_2 group native to its structure. This increased hydrophilicity aids in overcoming the $\pi-\pi$ stacking interaction between drugs and nanotubes while facilitating its detachment from the carrier. The release trend was just opposite for both MTX [Figure S4(c,d)] and PTX loaded CNTs. For MTX, the extent of drug release was higher at cytosolic pH compared to acidic pH. At pH 7.4, approximately 60−70% of MTX was released from the nanotubes within 24 h of incubation. The release rate was lowered to 35−45% at pH 5.5. The rate of drug release was even lower in the case of PTX [Figure S4(e,f)], as only 30−32% of the drug is released from f-CNTs after 48 h of incubation at pH 7.4. Because of the limited solubility of PTX in aqueous buffer, the release profile of PTX from the nanotubes was assessed under sink conditions using a 1:1 (v/v) mixture of methanol and PBS at 37 °C under constant stirring at 1200 rpm. The slow release of PTX from the nanotubes may be attributed to the strong hydrophobic interaction between PTX and CNTs. The observed release profiles suggest that MTX and PTX will act more efficiently if their respective carriers are localized in the cytoplasm.

Interaction of f-CNTs with Live Cells. As a preliminary step to comprehend the effect of surface functional molecules on the therapeutic performance of drug loaded CNTs, we sought to determine whether all f-CNTs (**1**−**6**) prepared in our study were able to interact with live cells. In line with that objective, both p- and f-CNTs **1**−**6**, fluorescently labeled with RITC, were allowed to interact with different cell types as shown in Table 1. All conditions including culture media, incubation time, and temperature were kept identical for all the formulations. In Table 1, representative confocal images of f-CNT internalized cells are shown for the preparations **1**−**6**. The "cell type" column enlists the different types of cell lines studied. Representative imaging data from these studies are included following interaction of f-CNTs (**1**−**6**) with adherent mammalian cell monolayers (A549, HeLa, or MCF7). The quantitative data for cellular internalization of f-CNTs have been supplemented as Figure S5 (Supporting Information). As is evident from these studies, all f-CNTs seemed to be capable of internalization by all cell types, revalidating that the functional groups present on surfaces of CNTs do not determine whether f-CNTs will be internalized by a particular cell type. Even p-CNTs lacking any distinct functionality on its surface showed internalization to some extent in all the cell lines. These results are in agreement with the findings of Kosteralos et al. according to which cellular uptake of f-CNTs is independent of their surface functionality and cell type.[4] In this

connection, it is worth noting that although CNTs, irrespective of their surface functionality, are internalized by cells, the extent of cell uptake is typically governed by the nature of functional groups associated with CNTs. Thus, both amine and carboxyl CNTs showed significantly higher uptake ($p < 0.01$) compared to p-CNTs. The uptake was further elevated in the case of FA and HA-CNTs. The observed differences were thought to be a consequence of differential cell−nanotube interaction regulating the internalization of f-CNTs inside their molecular target. Therefore, in the very next step, we tried to elucidate whether and how the cell internalization mechanism and subcellular translocation of f-CNTs depend on their surface functionality.

Surface Chemistry Dependent Internalization Pathway and Intracellular Trafficking of f-CNTs. In order to study the influence of endocytosis inhibiting conditions on the observed uptake and internalization of f-CNTs, NaN_3 pretreated A549 cells were incubated with p- and f-CNTs **1**−**6** for 3 h. Representative confocal images of A549 cells incubated with amino (**2**) and folate CNTs (**4**) have been presented as Figure 2A. Cell nuclei were stained with DAPI (blue fluorescence), while f-CNTs were labeled with RITC (red fluorescence). The quantitative data for cellular uptake of f-CNTs have been presented as Figure 2B. While blockage of energy-dependent pathway with NaN_3 had nominal influence on the cellular uptake of p-/f-CNTs **2** and **3**, the uptake of **1**, **4**, and **5** was significantly depreciated under similar conditions [Figure 2B(a)]. These results suggest the involvement of certain endocytic pathways in the cellular internalization of oxidized CNTs (**1**), FA-CNTs (**4**), HA-CNTs (**5**), and ES-CNTs (**6**) while **2** and **3** seemed to have internalized via passive diffusion. Of further note in this regard, cellular uptake of f-CNTs was independent of dose. An increase in CNT concentration from 5 to 20 μg/mL or NaN_3 concentration from 50 to 100 μg/mL had little or practically no influence on the extent of cellular uptake (data not shown). As specific ligands were conjugated to each of the preparations **4**, **5**, and **6**, it was necessary to elucidate whether any specific receptor is involved in the cellular internalization of the respective conjugates. Subsequently, A549 cells were incubated with **4**, **5**, and **6** in the absence and presence of 50 μg/mL free FA, HA, and ES, respectively. As evident from spectrofluorimetry based quantifications, cellular internalization of **4** was significantly inhibited in the presence of free FA while uptake of **5** and **6** remained unaltered under similar conditions [Figure 2B(b)]. Likewise, uptake of **5** was significantly inhibited in the presence of free HA while uptake of **4** and **6** was nominally affected under similar conditions. Representative flow cytograms of A549 and HeLa cells treated with RITC labeled FA-CNTs (**4**) have been depicted in Figure (2C). Cells pretreated with FA presented considerable depreciation in fluorescence intensity when compared to the untreated ones, suggesting a distinct role of folate receptor (FR) in the internalization of **4**. Similar observations were noted for HA-CNTs (**5**) as well (data not shown). In the case of ES-CNTs, although some changes in fluorescence intensity was observed in the presence of endocytic inhibitor and estradiol pretreatment, the effect of competitive inhibition was less significant than that of FA/HA-CNTs [Figure 2B(a,b)]. The observed difference may be easily explained if we take into consideration the intracellular localization and distribution of ERs. It is worthwhile to mention that classical ERs are mainly nucleocytoplasmic,[29,30] albeit some nonnuclear ER-αs are localized on the cell surface membrane as well. Consequently, blocking of ERs with excess of estradiol did not totally restrict the internalization of f-CNTs inside their target cells but altered their extent of cellular uptake and intracellular distribution. The confocal image of A549 cells exposed to **6** with and without ES treatment has been shown in Figure (2D). In the absence of endocytosis inhibitors, ES-CNTs showed significant propensity to localize in the nuclear and perinuclear region whereas for ES pretreated cells, the nanotubes were mainly restricted to cellular cytoplasm. The observation is consistent with the proposed mechanism of subcellular translocation of steroid hormones like estrogen. In general, steroid hormones are hydrophobic ligands that pass through the cellular membrane by passive diffusion and to some extent receptor mediated endocytosis driven by ligand−receptor binding interaction between steroids and their cell-surface localized cognate receptors. In the absence of excess estradiol, ES-CNTs can effectively bind with their cognate receptors, initiate conformational changes and release of molecular chaperone (Hsp 90, Hsp 70, cyclophilin, and p23) from the receptors,[31] activate them, and subsequently be transported to the nucleus via a genomic pathway. Blocking/saturation of ERs with excess estradiol does not allow the conjugate **6** to bind with the initially inactivated ERs (aporeceptors) and to initate the energy-dependent process required for transportation of nanotubes from cytoplasm to nucleus. Of note, internalization of **1** was nominally affected in the presence of free FA, HA, or ES, indicating the noninvolvement of any ligand-specific receptor. It seems that the negatively charged carboxyl functions on **1** indulge in nonspecific interactions with nonspecific receptors by electrostatic interaction of negative particles, especially scavenger receptor class B, type I (SR-BI), aberrantly expressed on the surface of A549 cells. In this regard, it may be further noted that although cell internalization of **1**, **4**, **5**, and **6** significantly deflated in the presence of endocytosis inhibitors, the internalization was not totally blocked. These observations suggest that even though surface functional molecules has a critical influence on the mechanistic pathway of the internalization of CNTs, the involvement of a nonspecific "nano-needle" mechanism cannot be overruled. As evident from Figure 2B(a), at least 20−30% of f-CNTs were internalized by cells via an energy-independent mechanism. Consequently, p-CNTs, which lack any distinct chemical functionality on their surface, were internalized to some extent in all the three cell lines suggesting the involvement of both energy independent and dependent pathways in the cellular internalization of f-CNTs. It is particularly important to note that differential mechanisms of cellular internalization may lead to different subcellular distribution of f-CNTs so that the same anticancer agent when delivered through different f-CNTs may result in different activities.

To understand the contribution of surface chemistry on the intracellular trafficking of CNTs, A549 cells were incubated with f-CNTs **1**−**6** and their colocalization with various cell organelles (lysosomes, mitochondria, and nucleus) was studied using confocal microscopy.[14] For lysosome and mitochondrial colocalization experiments, f-CNTs were covalently tagged with a near-infrared (NIR) dye AF-647 (indicated as gray fluorescence) whereas lysosomes and mitochondria were stained with Neutral Red (NR, red fluorescence) and rhodamine 123 (Rh123, green fluorescence), respectively. For nuclear colocalization analysis, CNTs were labeled with RITC (red fluorescence) while the nucleus was stained with 4′,6-diamidino-2-phenylindole (DAPI, blue fluorescence). The

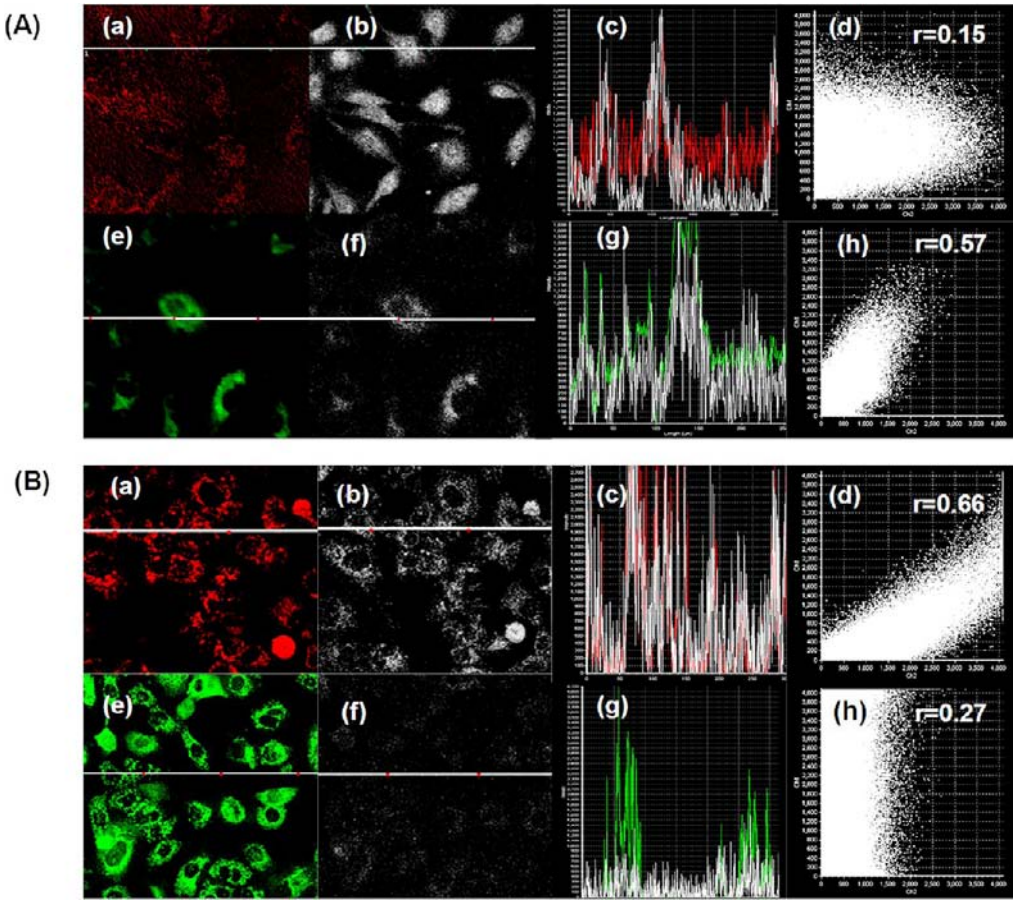

Figure 3. Representative confocal images of A549 cells treated with (A) amine CNTs, **2**, and (B) folate CNTs, **4**. For each incubation type, (a) and (b) represent the line display of AF647 and NR fluorescence, respectively. (c) Line profile analysis of (a) of AF647 and NR fluorescence. (d) Scatter plot of (b). (e, f) Line display of Rh123 and AF547 fluorescence. (g) Line profile analysis of AF647 and Rh123 fluorescence. (h) Scatter plot of (a), where the horizonatal and vertical axes of each line plot represent length and intensity of the line analyzed, and of (b), where the horizontal and vertical axes of each scatter plot represent the values of pixels in channel 2 (ch2) and channel 1(ch1), respectively.

variations in fluorescence intensity along a line were analyzed through line profile analysis, whereas colocalization in the entire field of view was determined by analysis of a scatter plot, generated with Olympus Fluoview software. The extent of colocalization between AF-647/RITC labeled CNTs and an organelle specific fluorescence dye was measured in terms of Pearson's correlation coefficient (r) which is calculated according to the equation

$$r = \frac{\sum_i (S1_i - S1_{aver})(S2_i - S2_{aver})}{\sqrt{[\sum_i (S1_i - S1_{aver})^2 \sum_i (S2_i - S2_{aver})^2]}} \quad \text{(Eq. 1)}$$

where S1 is the signal intensity of pixels in the first channel and S2 is the signal intensity of pixels in the second channel. $S1_{aver}$ and $S2_{aver}$ are the average values of pixels in the first and second channel, respectively. In Pearson's correlation, the average pixel intensity values are subtracted from the original intensity values. Subsequently, the value of Pearson's coefficient (r) ranges from −1 to 1, with a value of −1 representing a total lack of overlap between pixels from the images and with a value of 1 indicating perfect image registration. Accordingly, Pearson's coefficient $r \geq 0.5$ is generally considered as the indicator of good colocalization.[13] Figure 3 depicts the representative confocal micrographs of A549 cells incubated with selected f-CNTs preparations. As evident from the line display of AF-647 labeled **2** and NR stained lysosomes/Rh123 mitochondria (Figure 3A), amino-CNTs (**2**) presented appreciable colocalization with mitochondria (r = 0.54) and nominal proclivity to accumulate in lysosomes (r = 0.15). In contrast, FA-CNTs (**3**) showed significant lysosomal colocalization (r = 0.66) with minimal propensity toward mitochondrial compartmentalization (r = 0.27). The observed differences can be well-explained on the basis of different surface functionality associated with **2** and **4**. Because of the presence of free amine groups, the conjugate **2** presented a positive ζ potential (~9 ± 1 mV) at physiological pH, which possibly directed the conjugate **2** toward the negatively charged mitochondrial membrane, thereby facilitating its mitochondrial compartmentalization. The observations are in line with a recent report by Bakalova et al. wherein amino functionalized, non-cross-linked dendrimer coated quantum dots (QDs) with a ζ potential of 7 mV were shown to induce mitochondrial depolarization with significant loss in mitochondrial membrane potential ($\Delta\psi_m$) while QDs embedded in cross-linked, negatively charged carboxylated dendrimer presented no detectable change in mitochondrial potential.[32] At the same time, the lysosomal trafficking of FA-CNTs is in agreement with earlier reports according to which formation of ligand receptor complexes results in the formation of endocytic vesicles,[33] which in turn is believed to translocate the internalized conjugate from cell membrane to lysosomes. The lysosomal trafficking of HA-CNTs (**5**) (see Supporting Information Figure S6A) could be explained following a similar

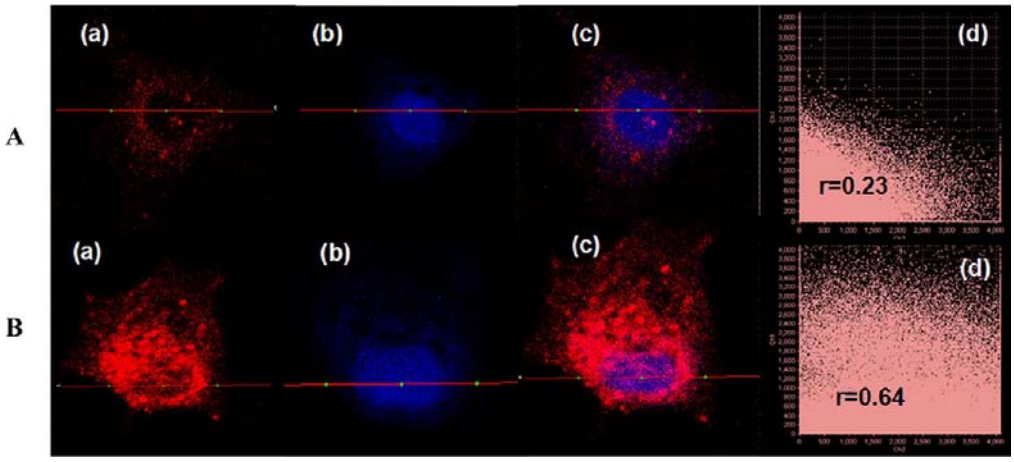

Figure 4. Representative confocal images of a single A549 cell treated with (A, top panel) folate CNT, **2**, and (B, bottom panel) estradiol CNT, **4**. For each incubation type, a, b, and c represent the line display of fluorescence signals of RITC, DAPI, and merged overlay of RITC/DAPI, respectively. (d) Scatter plot. The horizontal and vertical axes of each scatter plot represent the values of pixels in channel 2 (ch2) and channel 1 (ch1), respectively.

paradigm in which binding of HA to CD44 receptors was reasoned to facilitate their endolysosomal trafficking. We, however, did not observe any nuclear colocalization for either FA or HA-CNTs. Representative confocal images of RITC labeled FA-CNTs (**4**) and DAPI stained nuclei are presented in Figure 4A. Line display and scatter plot analyses validated that FA-CNTs are mainly distributed within the cellular cytoplasm, leaving a clear zone of the nucleus. Almost similar intracellular distribution was observed for carboxylated and PEGylated CNTs. Unlike Cheng et al.,[34] PEGylated CNTs, developed in course of our study, did not show any nuclear accumulation and was mainly confined to the cellular cytoplasm with partial colocalization in the mitochondria (see Supporting Information Figure S6B). The observed differences may be explained in terms of different end-functionality possessed by each f-CNT preparation. In their study, Cheng et al. used diamine terminated PEG, which might have rendered positive charges to the nanotubes, thereby facilitating their nuclear translocation. In contrast, PEGylated CNTs investigated in the present study were terminated with a methoxy ($-OCH_3$), which renders the nanotubes almost neutral (ζ potential of approximately -3 mV) at physiological pH. Other than surface functionality/charge considerations, the diameter of CNTs is a critical concern that determines their permeability across the nuclear membrane. As evident from scanning electron microscopy, the diameters of all f-CNTs (**1**−**6**) that had been investigated in this study ranged between 30 and 50 nm (representative image presented in Figure S7), which were too large to permeate across the nuclear pores (10−20 nm). Although f-CNTs **1**−**5** failed to cross the nuclear barrier, estradiol-CNTs (**6**) with a comparable diameter showed appreciable colocalization (r > 0.6) with the nucleus (Figure 4B). The results, though seemingly paradoxical, may be rationalized if we look into the cell internalization mechanism of estradiol-CNTs. The presence of an estradiol moiety on the surface of CNTs facilitates the binding of drug loaded CNTs with cytoplasmic ERs and facilitates their energy-dependent transport across the nuclear membrane. As reported in a number of studies, steroids have the unique capacity to dilate/perforate the nuclear pore through formation of nuclear pore complexes. A similar mechanism, however, is not operative for the other f-CNTs so that f-CNTs **1**−**5** were mostly localized in either cytosol or thecal organelles (lysosomes and mitochondria). The Pearson colocalization coefficients (r) of various f-CNTs with major cell organelles (lysosome, mitochondria, and nucleus) have been summarized in Table 3. A careful scrutiny of the data revalidates that transmembranal pathways of functionalized CNTs are critically surface chemistry dependent. In the present study, FA and HA tethered CNTs (**4**, **5**) presented appreciable colocalization with lysosomes (r > 0.5) while amine CNTs (**2**) and estradiol CNTs (**6**) were compartmentalized in mitochondria and nucleus, respectively. The fact that CNTs can be delivered into various subcellular compartments by conjugating with different functional molecules contributes a new tool for the development of organelle-specific, therapeutic vectors based on CNTs that can significantly enhance the therapeutic effect.

Table 3. Pearson's Colocalization Coefficient of Various f-CNTs with Various Cell Organelles

S/no.	formulation tested (drug/f-CNT)	Pearson's colocalization coefficient (r)		
		lysosome	mitochondria	nucleus
1	CNT-COOH	0.23 ± 0.05	0.12 ± 0.04	0.16 ± 0.02
2	CNT-NH_2	0.15 ± 0.04	0.54 ± 0.05	0.31 ± 0.06
3	CNT-PEG	0.08 ± 0.02	0.48 ± 0.05	0.23 ± 0.05
4	CNT-FA	0.66 ± 0.05	0.27 ± 0.03	0.23 ± 0.05
5	CNT-HA	0.64 ± 0.06	0.56 ± 0.02	0.22 ± 0.04
6	CNT-ES	0.19 ± 0.04	0.29 ± 0.04	0.64 ± 0.07

Effect of Surface Chemistry on the Cytotoxicity of Drug Loaded f-CNTs. Having correlated the surface functionality of f-CNTs with their intracellular trafficking, we tried to elucidate whether the cytotoxic potential of drug loaded CNTs (i−xxi) can be correlated with their surface chemistry. Subsequently, the cytotoxicity of all drug-loaded CNTs (i−xxi) was determined using the conventional MTT assay. The IC_{50} values of the formulations i−xxi in three different cell lines compared to free drugs have been summarized in Table 2. The dose response cytotoxicity curve for each formulation including free drugs has been provided in Supporting Information (Figure S6). In most of the cases, cytotoxicity exerted by each drug loaded f-CNTs was invariably higher than that of the free drug. It seemed that the intracellular availability of cytotoxic

Table 4. Quantification of f-CNT Induced Apoptosis in A549 Cells

S/no.	formulation tested	quantification of various apoptotic markers[a]				
		early apoptotic cells (%), AV (+ve)	late apoptotic cells (%), TUNEL	condensed nuclei (%), PI	fragmented nuclei (%), PI	fragmented DNA (%), DPA
1	control	2.0 ± 0.6[a]	5.2 ± 1.5[a]	5 ± 2[a]	8.17 ± 2.34[a]	1.98 ± 0.22[a]
2	ES-CNT-PTX	46.2 ± 5.8[b]	55.1 ± 8.7	60 ± 5	37.5 ± 4.5	37.5 ± 5.2
		a***	a***	a***	a***	a***
3	ES-CNT-DOX	85.7 ± 5.6	78.2 ± 7.8	75 ± 4	55.2 ± 6.5	57.5 ± 4.3
		a***, b**	a***, b*	a***, b*	a***, b**	a***, b**

[a]Data represent the mean ± SEM ($n = 3$). a* and b* represent quantification of various apoptotic markers with respect to ES-CNT-PTX ((***) $p < 0.001$, (**) $p < 0.01$, (*) $p < 0.05$).

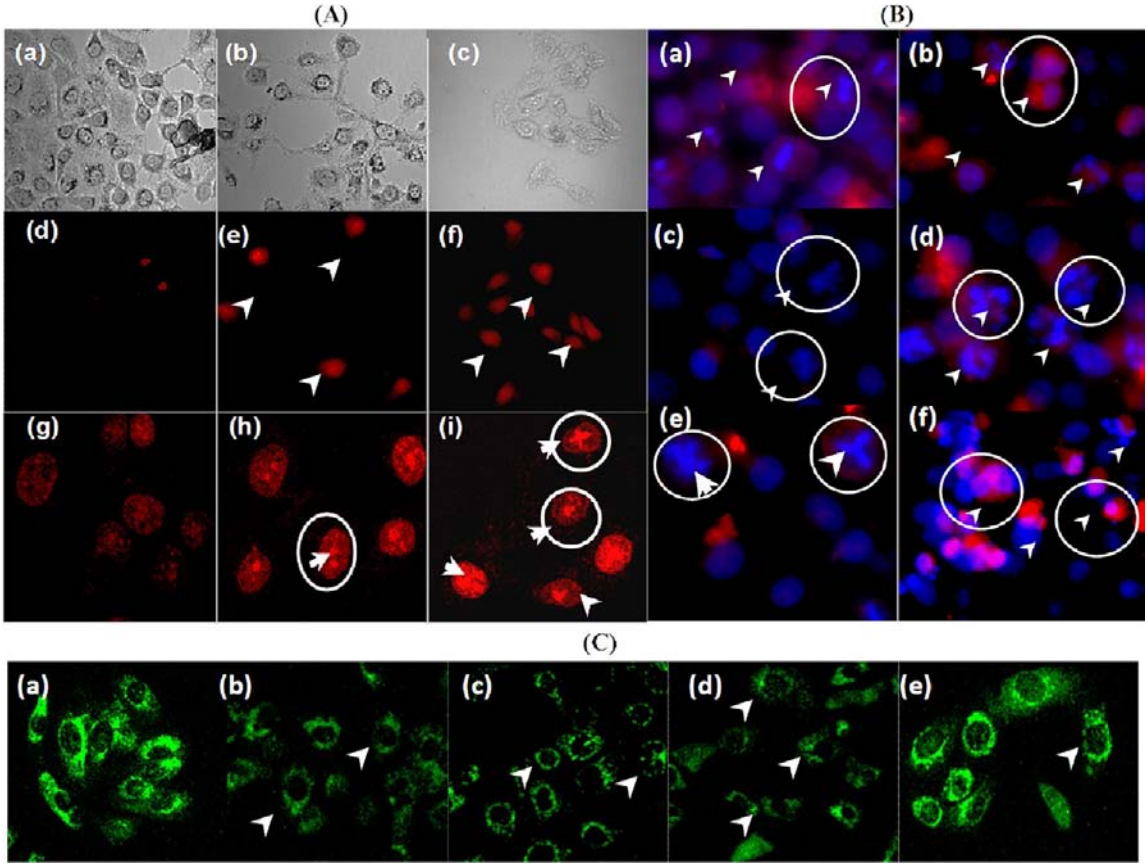

Figure 5. (A) Representative confocal images of A549 cells treated with (a, d, g) PBS (left panel), (b, e, h) estradiol-CNT-PTX (middle panel), and (c, f, i) estradiol-CNT-DOX (right panel). The upper left, middle, and right panels represent the DIC images of untreated/f-CNT treated cells (a–c), AV(+ve) cells (d–f) and representative fluorescence images of condensed/fragmented nuclei (g–i) stained with PI prior to imaging. The white arrows indicate cells in early and late apoptosis. (B) Representative fluorescence image of HeLa cells treated with (a, b) FA-CNT-PTX, (c, d) FA-CNT-DOX, and (e, f) FA-CNT-MTX for 6 h (left panel) and 24 h (right panel). The red fluorescence represents RITC (a, b)/DOX loaded f-CNTs, while blue represents DAPI stained nuclei. (No fluorescent label was required for DOX loaded CNTs, as the drug itself shows intrinsic red fluorescence.) The circle represents various hallmarks of apoptosis like condensed/fragmented nuclei and apoptotic bodies. (C) Mitochondrial depolarization of A549 cells treated with (a) control, (b) PEG-CNT-PTX, (c) HA-CNT-PTX, (d) CNT-NH_2-PTX, and (e) CNT-ES-PTX.

drugs delivered through f-CNTs was higher than that of the respective free drug, which in turn was believed to augment their cytotoxic activity. It was further interesting to observe that cytoxic responses to drug loaded CNTs was cell and surface-functionality specific, i.e., the same drug when delivered through different f-CNTs presented different activities. For example, in the HeLa cell line, which is known to overexpress folate and hyaluronate receptors, anticancer agents delivered through FA/HA-CNTs exhibited higher anticancer activity than the FA/HA nontargeted formulations (**1**–**3**). Similarly, in estrogen receptor (ER) overexpressing MCF7 cells, drugs delivered through ES-CNTs presented lower IC_{50} values than FA, HA, or PEGylated CNTs. In all the three cell lines, drugs delivered through p-CNTs exhibited the least antiproliferative activity, possibly because of their lower cellular internalization compared to the functionalized ones. For all the anticancer agents studied, cytotoxicity of ligand-anchored CNTs, in general, was significantly ($p < 0.05$) higher than plain carboxylated, aminated, or PEGylated CNTs. These results clearly indicate that cytotoxicity of the entrapped drug critically depends on the surface functionality associated with CNTs.

Correlation between Intracellular Trafficking and Cytotoxicity of Drug-Loaded f-CNTs. As subcellular trafficking of f-CNTs is critically influenced by their surface

chemistry, we tried to interpret the observed cytotoxicity profiles of various f-CNT-drug combinations i–xxi (Table 2) in light of their differential intracellular trafficking. A careful scrutiny of Table 2 reveals that MTX and DOX loaded ES-CNTs exhibits the highest cytotoxicity in A549 and MCF7 cells, followed by FA and HA-CNTs. The observed trend can be easily justified if we concentrate on the site of action of each drug molecule. MTX, being a folate antimetabolite, exerts its antitumor activity by interfering in the DNA biosynthetic pathway. The same is true for DNA intercalating drugs like DOX. As evident from intracellular trafficking studies (Figure 4B), estradiol CNTs concentrated mainly in the nucleus, which is also the site of action for both MTX and DOX. At this point, it may be noted that both A549 and MCF7 cells express very high levels of ER-α [35] in contrast to ER(−ve) HeLa cells.[36] Hence, the energy dependent pathway that is responsible for the translocation of ES-CNTs (**6**) from cytoplasm to nucleus is not operative in HeLa cells. Subsequently, the IC_{50} of MTX/DOX loaded ES-CNTs in HeLa cells is almost double the activity of the therapeutic conjugates in either A549 or MCF7 cells. For MTX delivery, FA-CNTs also showed appreciable activity in all the three cell lines and the observed cytotoxicity was almost comparable to that of ES-CNTs. Although FA-CNTs did not colocalize with the nucleus, the conjugate was internalized by cells though FR mediated endocytosis (Figure 2B and Figure 2C), which in turn augmented the intracellar concentration of the therapeutic conjugate and facilitated its colocalization with lysosomes. It might be that FA-CNTs (**3**) were initially translocated to low pH (4.5–5.5) lysosomes (Figure 3B) via the endolysosomal pathway wherein the amide bond between FA and carboxylated CNTs was hydrolyzed chemoenzymatically to rejuvenate the surface amine groups. Such cationization possibly facilitated the fusion of CNTs with endosomes, their escape into the cytosol via proton sponge effect, and subsequent drug release to exert therapeutic action on the nuclei. Likewise, the high anticancer activity of DOX loaded FA/HA CNTs was attributed to their intrinsic proclivity toward lysosomal accumulation.[13] Unlike MTX and DOX, PTX has a nominal effect on nucleus. Therefore, encapsulation of PTX within ES-CNTs did not significantly alter the therapeutic performance of ES-CNT/PTX combinations when compared to free drug. For PTX delivery, the highest cytotoxicity was executed by PTX-loaded HA-CNTs, closely followed by amine-functionalized and PEGylated CNTs, all of which showed significant propensity toward mitochondrial colocalization. As PTX itself acts directly on mitochondria, it is very likely that any f-CNT preparation that delivers the drug selectively to mitochondria will show higher therapeutic activity compared to those meant for targeting other organelles. To elucidate this effect, A549 cells were incubated with two different f-CNT-drug combinations (Es-CNT-DOX and Es-CNT-PTX) and the various hallmarks of apoptosis (phosphatidylserine (PS) externalization, mitochondrial depolarization, nuclear condensation, and DNA fragmentation) were studied qualitatively and quantitatively using annexinn V (AV)-Cy3 apoptosis detection kit, Rh123 staining, propidium iodide (PI) staining, and TUNEL and DPA assays (Table 4). Representative DIC and fluorescence images of A549 cells incubated with Es-CNT-DOX and Es-CNT-PTX (in a concentration normalized to 1 μg/mL free DOX/PTX) have also been presented in Figure 5A(a–f). PS, which is present on the cytoplasmic side of the cell membrane, is externalized during apoptosis.[37] Externalized PS binds with annexin V (AV) and gives red fluorescence. As evident from Figure 5A(a–f) and Table 4, cells incubated with ES-CNT-DOX presented significantly higher ($p < 0.01$) number of PS externalized (AV +ve) cells (85.7 ± 8.7%) compared to Es-CNT-PTX (46.2 ± 5.8%). Likewise, nuclear condensation and fragmentation were more severe for Es-DOX-CNT treated cells [Figure 5A(g–i)] when compared to their corresponding PTX loaded counterpart. As evident from the results, Es-CNT-DOX could induce apoptosis more efficiently than Es-CNT-PTX, revalidating the importance of subcellular distribution of f-CNTs on the therapeutic performance of the loaded cytotoxin. To further strengthen our inference, HeLa cells were incubated with three more CNT–drug combinations (FA-CNT-PTX, FA-CNT-MTX, and FA-CNT-DOX) in a concentration normalized to 5 μg/mL free drug and apoptosis was studied. Figure 5B presents the fluorescence images of HeLa cells treated with the proposed formulations for 6 and 24 h. For all three formulations, apoptosis was initiated as early as 6 h. However, the effect was less pronounced for the f-CNT/PTX combination. In line with our cytotoxicity results, both FA-CNT-DOX and FA-CNT-MTX showed a higher number of condensed and fragmented nuclei compared to their PTX loaded counterpart (Figure 5B). As shown in Figure S4(a–f), the release of PTX from FA-CNTs is strongly disfavored under lysosomal conditions (pH 5.5), which might be the most plausible reason for the lower activity of PTX bound FA-CNTs compared to its MTX/DOX loaded congener. Interestingly, PTX delivered through HA-CNTs and amine-CNTs showed considerably higher dissipation in mitochondrial membrane potential compared to FA/ES-CNTs (Figure 5C), which suggests that the efficacy of any drug loaded CNT platform is critically dependent on the cell internalization pathway and subcellular distribution of the therapeutic vector. As cell internalization and intracellular trafficking of CNTs are closely associated with their surface chemistry, functional molecules associated with the surface of CNTs play a key role in determining the efficacy of any drug loaded CNT-platform. In this regard, it is worth mentioning that surface characteristics of f-CNTs such as hydrophobicity/hydrophilicity, surface charge, and chemical composition depend invariably on the organic molecules associated with their surface. Consequently, a small change in surface chemistry can significantly transform the binding avidity and their interactions with living cells/tissues, which in turn have a far-reaching influence on third order (intracellular) targeting. Because of the chemoenzymatic heterogeneity of the intracellular milieu, it may be assumed that chemical entity present on the surface of CNTs will show differential interactions with different organelles. In such a scientific panorama, the encapsulated drug has to primarily depend on its carrier and its surface chemistry for transporation to its target organelle, wherein the drug molecule is anticipated to detach from its respective carrier and exert the desired therapeutic activity.

■ CONCLUSION

We have successfully established that internalization, subcellular translocation, and cytotoxic responses to drug loaded CNTs can be effectively modulated by intelligent manipulation of surface functionality and associated linkers. For the first time, we embarked on the possibility of using a surface chemistry dependent switch to regulate or to remote-control the targeting and therapeutic efficacy of CNT-based theranostic platforms. The fact that internalization pathway and subcellular translocation of CNTs could be modulated by conjugating with

different functional molecules opens a new window for receptor and organelle-specific drug delivery in which a therapeutic module of interest can be specifically homed to its target organelle to augment the therapeutic effect. Finally, even though we have concentrated on a surface chemistry based "switch" for regulating the trafficking and performance of drug loaded f-CNTs inside cells, the possibility of fine-tuning their therapeutic activity by engineering their length, diameter, or physical forms needs to be explored. Overall, these findings not only improve our current understanding of the interaction of drug loaded f-CNTs and living cells but also pave the way to nanorobotic manipulation of theranostic CNTs based on surface chemistry modulation, which in turn is expected to benefit the development of futuristic nanobots for cancer theranostics.

■ ASSOCIATED CONTENT

Ⓢ Supporting Information

Transmission micrographs, FTIR and NMR spectra, in vitro release profile, in vitro cellular uptake data, subcellular distribution data, and dose response curves. This material is available free of charge via the Internet at http://pubs.acs.org.

■ AUTHOR INFORMATION

Corresponding Author

*Phone: +91172-2292055. Fax: +91172-2214692. E-mail: sanyogjain@niper.ac.in and sanyogjain@rediffmail.com.

Author Contributions

[†]M.D. and R.P.S. contributed equally.

Notes

The authors declare no competing financial interest.

■ ACKNOWLEDGMENTS

Financial support for this work was provided by Indian Council of Medical Research (ICMR, Grant 35/28/2010/-BMS), Government of India (GOI), New Delhi, India. M.D. and R.P.S. are grateful to Department of Science and Technology (DST), GOI, New Delhi, India, for providing postdoctoral and senior research fellowships, respectively. Director NIPER is acknowledged for providing necessary infrastructural facilities. Thanks are due to Bhupindar Kaur, Department of Anatomy, PGI Chandigarh, India, and Dr. Ravi S. Amarpati, SAIF, Central Drug Research Institute (CDRI, Lucknow), India, for assistance with flow cytometry and HRMAS-NMR analysis. The technical assistance of D. S. Chauhan and R. R. Mahajan is highly appreciated.

■ REFERENCES

(1) Bianco, A., Kostarelos, K., and Prato, M. (2008) Opportunities and challenges of carbon-based nanomaterials for cancer therapy. *Expert Opin. Drug Delivery 5*, 331−342.

(2) Thakare, V. S., Das, M., Jain, A. K., Patil, S., and Jain, S. (2010) Carbon nanotubes in cancer theragnosis. *Nanomedicine 5*, 1277−1301.

(3) Pastorin, G. (2009) Crucial functionalizations of carbon nanotubes for improved drug delivery: a valuable option? *Pharm. Res. 26*, 746−769.

(4) Kostarelos, K., Lacerda, L., Pastorin, G., Wu, W., Wieckowski, S., Luangsivilay, J., Godefroy, S., Pantarotto, D., Briand, J. P., and Muller, S. (2007) Cellular uptake of functionalized carbon nanotubes is independent of functional group and cell type. *Nat. Nanotechnol. 2*, 108−113.

(5) Bussy, C., Alexiou, C., Petros, R. A., Nystrom, A. M., Methven, L., and Kostarelos, K. (2012) Therapeutic Applications. In *Adverse Effects of Engineered Nanomaterials: Exposure, Toxicology, and Impact on Human Health* (Fadeel, B., Pietroiusti, A., Shvedova, A. A., Eds.) p 285, Elsevier, London.

(6) Raffa, V., Ciofani, G., Vittorio, O., Riggio, C., and Cuschieri, A. (2010) Physicochemical properties affecting cellular uptake of carbon nanotubes. *Nanomedicine 5*, 89−97.

(7) Lamm, M. H., and Ke, P. C. (2010) Cell trafficking of carbon nanotubes based on fluorescence detection. *Methods Mol. Biol. 625*, 135−151.

(8) Al-Jamal, K. T., Nerl, H., Müller, K. H., Ali-Boucetta, H., Li, S., Haynes, P. D., Jinschek, J. R., Prato, M., Bianco, A., and Kostarelos, K. (2011) Cellular uptake mechanisms of functionalised multi-walled carbon nanotubes by 3D electron tomography imaging. *Nanoscale 3*, 2627−2635.

(9) Kang, B., Chang, S., Dai, Y., Yu, D., and Chen, D. (2010) Cell response to carbon nanotubes: size-dependent intracellular uptake mechanism and subcellular fate. *Small 6*, 2362−2366.

(10) Mu, Q., Broughton, D. L., and Yan, B. (2009) Endosomal leakage and nuclear translocation of multiwalled carbon nanotubes: developing a model for cell uptake. *Nano Lett. 9*, 4370−4375.

(11) Lacerda, L., Russier, J., Pastorin, G., Herrero, M. A., Venturelli, E., Dumortier, H., Al-Jamal, K. T., Prato, M., Kostarelos, K., and Bianco, A. (2012) Translocation mechanisms of chemically functionalised carbon nanotubes across plasma membranes. *Biomaterials 33*, 3334−3343.

(12) Zhou, F., Xing, D., Wu, B., Wu, S., Ou, Z., and Chen, W. R. (2010) New insights of transmembranal mechanism and subcellular localization of noncovalently modified single-walled carbon nanotubes. *Nano Lett. 10*, 1677−1681.

(13) Datir, S. R., Das, M., Singh, R., and Jain, S. (2012) Hyaluronate tethered, "smart" multiwalled carbon nanotubes for tumor-targeted delivery of doxorubicin. *Bioconjugate Chem. 23*, 2201−2213.

(14) Swarnakar, N. K., Jain, A. K., Singh, R. P., Godugu, C., Das, M., and Jain, S. (2011) Oral bioavailability, therapeutic efficacy and reactive oxygen species scavenging properties of coenzyme Q10-loaded polymeric nanoparticles. *Biomaterials 32*, 6860−6874.

(15) Singh, R., Das, M., Thakre, V., and Jain, S. (2012) Functionalization density dependent toxicity of oxidized multiwalled carbon nanotubes in a murine macrophage cell line. *Chem. Res. Toxicol. 25*, 2127−2137.

(16) Jain, S., Thakare, V. S., Das, M., Godugu, C., Jain, A. K., Mathur, R., Chuttani, K., and Mishra, A. K. (2011) Toxicity of multiwalled carbon nanotubes with end defects critically depends on their functionalization density. *Chem. Res. Toxicol. 24*, 2028−2039.

(17) Osorio, A. G., Silveira, I. C. L., Bueno, V. L., and Bergmann, C. P. (2008) $H_2SO_4/HNO_3/HCl$—functionalization and its effect on dispersion of carbon nanotubes in aqueous media. *Appl. Surf. Sci. 255*, 2485−2489.

(18) Pompeo, F., and Resasco, D. E. (2002) Water solubilization of single-walled carbon nanotubes by functionalization with glucosamine. *Nano Lett. 2*, 369−373.

(19) Das, M., Mishra, D., Maiti, T. K., Basak, A., and Pramanik, P. (2008) Bio-functionalization of magnetite nanoparticles using an aminophosphonic acid coupling agent: new, ultradispersed, iron-oxide folate nanoconjugates for cancer-specific targeting. *Nanotechnology 19*, 415101.

(20) Jain, S., Mathur, R., Das, M., Swarnakar, N. K., and K., M. A. (2011) Synthesis, pharmacoscintigraphic evaluation and antitumor efficacy of methotrexate loaded, folate conjugated, stealth albumin nanoparticles. *Nanomedicine 6*, 1733−54.

(21) Lay, C. L., Liu, H. Q., Tan, H. R., and Liu, Y. (2010) Delivery of paclitaxel by physically loading onto poly (ethylene glycol)(PEG)-graftcarbon nanotubes for potent cancer therapeutics. *Nanotechnology 21*, 065101.

(22) Das, M., Bandyopadhyay, D., Mishra, D., Datir, S., Dhak, P., Jain, S., Maiti, T. K., Basak, A., and Pramanik, P. (2011) Clickable, trifunctional magnetite nanoparticles and their chemoselective biofunctionalization. *Bioconjugate Chem. 22*, 1181−1193.

(23) Bruce, I. J., and Sen, T. (2005) Surface modification of magnetic nanoparticles with alkoxysilanes and their application in magnetic bioseparations. *Langmuir 21*, 7029−7035.
(24) Das, M., Mishra, D., Dhak, P., Gupta, S., Maiti, T. K., Basak, A., and Pramanik, P. (2009) Biofunctionalized, phosphonate grafted, ultrasmall iron oxide nanoparticles for combined targeted cancer therapy and multimodal imaging. *Small 5*, 2883−2893.
(25) Jain, A. K., Swarnakar, N. K., Das, M., Godugu, C., Singh, R. P., Rao, P. R., and Jain, S. (2011) Augmented anticancer efficacy of doxorubicin loaded polymeric nanoparticles after oral administration in breast cancer induced animal model. *Mol. Pharmaceutics 8*, 1140−51.
(26) Von Knethen, A., and Brune, B. (1997) Cyclooxygenase-2: an essential regulator of NO-mediated apoptosis. *FASEB J. 11*, 887.
(27) Jain, A. K., Swarnakar, N. K., Godugu, C., Singh, R. P., and Jain, S. (2011) The effect of the oral administration of polymeric nanoparticles on the efficacy and toxicity of tamoxifen. *Biomaterials 32*, 503−15.
(28) Das, M., Bandyopadhyay, D., Singh, R., Harde, H., Kumar, S., and Jain, S. (2012) Orthogonal biofunctionalization of magnetic nanoparticles via "clickable" poly(ethylene glycol) silanes: a "universal ligand" strategy to design stealth and target-specific nanocarriers. *J. Mater. Chem. 22*, 24652−24667.
(29) Ariazi, E. A., Ariazi, J. L., Cordera, F., and Jordan, V. C. (2006) Estrogen receptors as therapeutic targets in breast cancer. *Curr. Top. Med. Chem. 6*, 181−202.
(30) Maggiolini, M., and Picard, D. (2010) The unfolding stories of GPR30, a new membrane-bound estrogen receptor. *J. Endocrinol. 204*, 105−114.
(31) Rai, S., Paliwal, R., Vaidya, B., Gupta, P. N., Mahor, S., Khatri, K., Goyal, A. K., Rawat, A., and Vyas, S. (2007) Estrogen(s) and analogs as a non-immunogenic endogenous ligand in targeted drug/DNA delivery. *Curr. Med. Chem. 14*, 2095−2109.
(32) Bakalova, R., Zhelev, Z., Kokuryo, D., Spasov, L., Aoki, I., and Saga, T. (2011) Chemical nature and structure of organic coating of quantum dots is crucial for their application in imaging diagnostics. *Int. J. Nanomed. 6*, 1719.
(33) Pandey, M. S., Harris, E. N., Weigel, J. A., and Weigel, P. H. (2008) The cytoplasmic domain of the hyaluronan receptor for endocytosis (HARE) contains multiple endocytic motifs targeting coated pit-mediated internalization. *J. Biol. Chem. 283*, 21453.
(34) Cheng, J., Fernando, K. A. S., Veca, L. M., Sun, Y. P., Lamond, A. I., Lam, Y. W., and Cheng, S. H. (2008) Reversible accumulation of PEGylated single-walled carbon nanotubes in the mammalian nucleus. *ACS Nano 2*, 2085−2094.
(35) Hsieh, C. Y., Santell, R. C., Haslam, S. Z., and Helferich, W. G. (1998) Estrogenic effects of genistein on the growth of estrogen receptor-positive human breast cancer (MCF-7) cells in vitro and in vivo. *Cancer Res. 58*, 3833−3838.
(36) Maggiolini, M., Bonofiglio, D., Marsico, S., Panno, M. L., Cenni, B., Picard, D., and Andò, S. (2001) Estrogen receptor α mediates the proliferative but not the cytotoxic dose-dependent effects of two major phytoestrogens on human breast cancer cells. *Mol. Pharmacol. 60*, 595−602.
(37) Vermes, I., Haanen, C., Steffens-Nakken, H., and Reutellingsperger, C. (1995) A novel assay for apoptosis flow cytometric detection of phosphatidylserine expression on early apoptotic cells using fluorescein labelled annexin V. *J. Immunol. Methods 184*, 39−51.